Experimental investigations of absorption and dispersion profiles of a strongly driven transition: V-shaped three-level system with a strong probe

Changjiang Wei,* Neil B. Manson, and John P. D. Martin
Laser Physics Centre, Research School of Physical Sciences and Engineering, Australian National University, Canberra, Australian Captital Territory 0200, Australia
(Received 28 April 1994)

This paper reports on experimental investigations of absorption, dispersion, and amplitude profiles of the Autler-Townes doublet in a V-shaped three-level system where the probe field intensities varied from weak to strong. The experiments were carried out on the ground-state hyperfine transitions of the nitrogen-vacancy color center in diamond using the Raman heterodyne technique, a sensitive optically detected magnetic resonance technique. A strong pump field is on resonance with the $I_z=|0\rangle \Longleftrightarrow |1\rangle$ transition at 4.7 MHz and the resultant Autler-Townes profiles are probed with a separate field scanning through the $I_z=|0\rangle \Longleftrightarrow |-1\rangle$ transition at 5.4 MHz. As the probe power increases the absorptive profile of the Autler-Townes doublet becomes saturated and power broadened and the two components overlap constructively. In contrast, the inner parts of the two dispersive doublet components interfere destructively due to a π phase difference. The amplitude profile has an anomalous line shape at high probe intensity due to the different saturation behaviors of the absorptive and dispersive components. The experimental profiles are in good agreement with theoretical profiles calculated by solving the equation of motion of the density matrix under the steady-state limit.

PACS number(s): 42.50.Hz, 42.62.Fi, 32.80.Bx, 32.30.Dx

I. INTRODUCTION

Previously, we have reported experimental investigations of the absorption and dispersion responses of a strongly driven two-level system when probed by a weak [1] and a strong [2] field in a nuclear magnetic resonance (NMR) transition. The levels are two out of the three hyperfine levels associated with a nuclear spin of $I=1$ within the ^3A ground state of the nitrogen-vacancy (N-V) center in diamond (see Fig. 1). Both the pump and the probe field interact with the $I_z=|0\rangle \Longleftrightarrow |-1\rangle$ transition at 5.4 MHz. This nuclear spin system has also previously been the subject of a separate study where all the three levels are involved; one transition (the $I_z=|0\rangle \Longleftrightarrow |1\rangle$ transition at 4.7 MHz) was driven by a strong field and a second transition (the $I_z=|0\rangle \Longleftrightarrow |-1\rangle$ transition at 5.4 MHz) was probed by a weak field [3]. For completeness, in this work, the study of this three-level system is extended to the situation where the probe field is also strong. This study is worthwhile in that it reports absorption and dispersion measurements of a three-level system interacting with two electromagnetic fields where both pump and probe fields are strong.

The splitting of a level by a strong driving field, known as the dynamic (ac) Stark splitting or Autler-Townes effect [4], is the manifestation of the interaction of monochromatic electromagnetic fields with matter and has been studied by many researchers [1–25] both theoretically and experimentally. Such experimental studies provide important and fundamental information about the nature of radiation-matter interactions and can be compared directly with theoretical calculations. However, in most earlier studies including our own [3], the situations

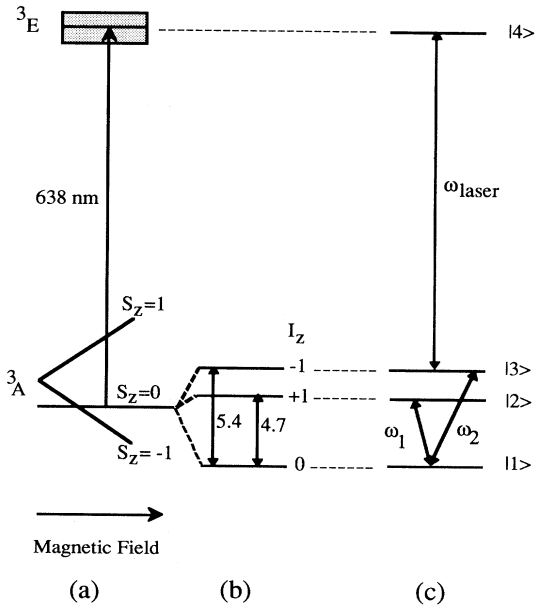

FIG. 1. Schematic of energy levels of the hyperfine structures within the ^3A ground state of the N-V center for an axial magnetic field. (a) Energy-level splitting of the ^3A ground state in a static magnetic field applied along the [111] axis; anticrossing occurs at 0.1028 T. (b) The hyperfine splitting at magnetic field slightly larger than 0.1028 T. (c) A V-shaped three-level system interacting with two rf fields.

*Present address: Department of Physics and Mathematical Physics, The University of Adelaide, Adelaide, South Australia 5005, Australia.

are restricted to the weak probe field limit [3–11,13–16] where the power of the probe field is kept sufficiently low that the interaction is linear and need only be treated to first order. For the strong probe field case where the probe field interaction is nonlinear, we are aware of only two reported investigations [12,17]. Gray and Stroud [12] reported the first observation of the power broadened Autler-Townes profiles with a sodium atomic beam as the three-level system. More recently Fisk, Bachor, and Sandeman [17] presented a systematic investigation of power broadened Autler-Townes profiles in a barium atomic beam. The sodium or barium atoms systems are interesting systems, but are not simple three-level systems due to hyperfine structure and the presence of isotopes. In both experiments the profiles are obtained by monitoring the fluorescence induced by the probe field, which is directly related to the diagonal term of the density matrix or the population of the fluorescent level [12,17]. The present work is different in that the off-diagonal term of the density matrix can be measured, giving the absorption and dispersion response profiles.

II. NITROGEN-VACANCY CENTER

This paper reports the experimental investigations of the absorption, dispersion, and amplitude profiles of a NMR three-level system interacting with two monochromatic electromagnetic fields. A strong rf pump field ω_1 is held fixed on resonance with the transition $|1\rangle \Longleftrightarrow |2\rangle$ and a rf probe field ω_2 probes the transition between $|1\rangle \Longleftrightarrow |3\rangle$ (Fig. 2). The pump field intensity is strong and kept fixed while the probe field intensity is varied from weak to strong.

The experiments involve NMR transitions in the ^3A electronic spin triplet ground state of the N-V center in diamond and the NMR transitions are detected by the Raman heterodyne method [26–28], a sensitive coherent optically detected magnetic resonance technique. The N-V center consists of a substitutional nitrogen atom accompanied by a carbon vacancy at a nearest-neighbor site [29,30]. The defect has a C_{3v} symmetry with the C_3 axis lying along the nitrogen-vacancy pair, which is the crystallographic [111] direction. There are four orientations

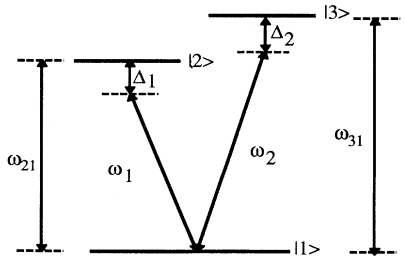

FIG. 2. Three-level system interacting with the two monochromatic applied fields. The strong pump field has frequency ω_1, detuning $\Delta_1=\omega_{21}-\omega_1$, and Rabi intensity χ_1. The probe field has frequency ω_2, detuning $\Delta_2=\omega_{31}-\omega_2$, and Rabi intensity χ_2.

of trigonal centers in the cubic lattice. At zero field the ^3A ground state is split by the crystal-field interaction into an electronic spin double $S_z=|\pm1\rangle$ and an electronic spin singlet $S_z=|0\rangle$ separated by 2.88 GHz [30–32]. When a static magnetic field is applied along the [111] direction, the magnetic field is axial for one orientation of the N-V centers whose C_3 axes lie along the [111] direction and only these aligned N-V centers are considered in this study. The magnetic field splits the $S_z=|\pm1\rangle$ electronic spin doublet. At a field of 0.1028 T the $S_z=|0\rangle$ and the $S_z=|-1\rangle$ levels anticross. The experiments were carried out with a magnetic field applied along the [111] direction close to level anticrossing region. The typical static magnetic field value used in experiments was $\sim$0.1050 T. The hyperfine interaction is associated with the nitrogen nuclear spin $I=1$ and the specific NMR transitions studied are those associated with the $S_z=|0\rangle$ electronic spin level. The energy levels and the optical and magnetic transitions involved in the experiments are shown in Fig. 1. The pump field was held fixed at the frequency of the $I_z=|0\rangle \Longleftrightarrow |1\rangle$ 4.7-MHz transition and the probe field was swept about the resonance frequency of the $I_z=|0\rangle \Longleftrightarrow |-1\rangle$ 5.4-MHz transition. The features of the NMR transition that make it suitable for studying the interaction with strong electromagnetic fields have been discussed previously [1,2]. Briefly, the main features of the system are the following: (i) the NMR transitions have large magnetic dipole transition moments due to the electronic spin wave-function mixing occurring in the level anticrossing region, (ii) because of the wave-function mixing optical transitions are allowed to a common excited state necessary for NMR transitions to be detected by the very sensitive Raman heterodyne technique, and (iii) the NMR transitions have only a small inhomogeneous broadening and the ratio of the inhomogeneous linewidth $\Gamma_{\rm inh}$ to the homogeneous linewidth $\Gamma_{\rm h}$ is about 3–4.

III. EXPERIMENT

The experimental arrangement is identical to those described in our other papers [1,2] and has been discussed elsewhere [3,28]. Raman heterodyne detection utilizes optical transitions by which the coherence between NMR transitions is probed. Therefore, in our experimental configuration four levels (three correspond to NMR and one to optical transition) and three fields (one optical and two rf fields) are involved. However, the power of the laser field is kept so low that it can be treated to the first order and it has been shown [27] that in this weak optical field limit the problem becomes a three NMR levels interacting with two rf fields.

The diamond crystal was mounted in the center of a six-turn rf coil and cooled to liquid-helium temperature (4.2 K). The static magnetic field applied along the [111] crystallographic direction was set to a magnitude close to the level anticrossing ($\sim$0.1050 T). The magnetic transition in the ^3A ground state was driven by the rf field with a magnitude on the order of 1 G. The output of a Coherent CR 599-21 cw, single-mode dye laser was fo-

cused on the sample. The laser frequency was tuned to the optical zero phonon line of the $^3A \Longleftrightarrow {}^3E$ transition at 638 nm and the laser power was on the order of 1 mW. The Raman heterodyne signal in the light transmitted through the crystal was detected by a photodiode [1,2]. The Raman heterodyne signal has a component in phase with the applied rf field and one out of phase with the applied rf field [27]. By solving the density-matrix equation of motion for the Raman heterodyne process it has been shown [27] that the in-phase and the out-of-phase signals are directly related to the real and the imaginary part of the off-diagonal term of the density matrix, respectively. In experiments the in-phase and the out-of-phase signals can be selected by adjusting the phase of the local oscillator (see Fig. 3 in [1]). In the amplitude profile measurements (see Fig. 2 in [2]) the output signal from the photodiode is directly fed into a spectrum analyzer. The amplitude signal is the vector sum of in-phase and out-of-phase components. The in-phase signal is referred as to the dispersion signal and the experimental traces are compared with theoretical calculations of the real part of the off-diagonal density-matrix element; likewise the out-of-phase signal is termed the absorption signal and compared with theoretical calculations of the imaginary part of the off-diagonal density matrix element as a function of applied rf field frequency.

IV. THEORY

A three-level system interacting with two near-resonant fields is shown in Fig. 2. The three-level system has energy levels $E_1 < E_2 < E_3$, corresponding to the three states $|1\rangle$, $|2\rangle$, and $|3\rangle$. The system interacts with two near-resonant fields of frequencies ω_1 and ω_2 where the rf magnetic field has the form

$$B_{\rm rf}(t) = B_1 \cos\omega_1 t + B_2 \cos\omega_2 t \ . \tag{1}$$

The Hamiltonians for this system can be written as

$$H = H_0 + H_I \ , \tag{2}$$

where H_0 is the atomic Hamiltonian and satisfies the eigenvector equation

$$H_0|m\rangle = E_m|m\rangle, \quad m = 1,2,3 \ . \tag{3}$$

H_I denotes the interaction of the three-level system with the electromagnetic fields and can be written in terms of the magnetic dipole interaction and in the near-resonant field approximation as

$$H_I = \begin{bmatrix} 0 & -2\hbar V_1 \cos\omega_1 t & -2\hbar V_2 \cos\omega_2 t \\ -2\hbar V_1 \cos\omega_1 t & 0 & 0 \\ -2\hbar V_2 \cos\omega_2 t & 0 & 0 \end{bmatrix} , \tag{4}$$

where V_1 and V_2 are defined by the Rabi frequencies χ_1 and χ_2 of the pump and the probe field, respectively.

$$\chi_1 \equiv 2V_1 = \frac{\mu_{21} B_1}{\hbar}, \quad \chi_2 \equiv 2V_2 = \frac{\mu_{31} B_2}{\hbar} \ . \tag{5}$$

The time evolution of the density matrix is given by

$$i\hbar \frac{\partial \rho}{\partial t} = [H,\rho] + (\text{relaxation terms}) \ . \tag{6}$$

where the rapidly oscillating factors of the off-diagonal elements can be removed by the transformations

$$\rho_{31} = \tilde{\rho}_{31} e^{-i\omega_2 t} \ , \tag{7a}$$

$$\rho_{21} = \tilde{\rho}_{21} e^{-i\omega_1 t} \ , \tag{7b}$$

$$\rho_{32} = \tilde{\rho}_{32} e^{-i(\omega_2 - \omega_1)t} \ . \tag{7c}$$

and the transition frequencies ω_{ij} and detunings Δ_1, Δ_2 are defined

$$\hbar\omega_{ij} = E_i - E_j \ , \tag{8a}$$

$$\Delta_1 = \omega_{21} - \omega_1 \ , \tag{8b}$$

$$\Delta_2 = \omega_{31} - \omega_2 \ , \tag{8c}$$

$$\Delta = \Delta_1 - \Delta_2 \ . \tag{8d}$$

The equation of motion of the density matrix in the rotating-wave approximation is given by

$$\frac{\partial \rho_{11}}{\partial t} = iV_1(\tilde{\rho}_{21} - \tilde{\rho}_{12}) + iV_2(\tilde{\rho}_{31} - \tilde{\rho}_{13}) - \frac{\rho_{11} - \rho_{11}^{\rm eq}}{T_1} \ , \tag{9a}$$

$$\frac{\partial \rho_{22}}{\partial t} = -iV_1(\tilde{\rho}_{21} - \tilde{\rho}_{12}) - \frac{\rho_{22} - \rho_{22}^{\rm eq}}{T_1} \ , \tag{9b}$$

$$\frac{\partial \rho_{33}}{\partial t} = -iV_2(\tilde{\rho}_{31} - \tilde{\rho}_{13}) - \frac{\rho_{33} - \rho_{33}^{\rm eq}}{T_1} \ , \tag{9c}$$

$$\frac{\partial \tilde{\rho}_{31}}{\partial t} l = -\left[\frac{1}{T_2} + i\Delta_2\right]\tilde{\rho}_{31} - iV_1\tilde{\rho}_{32} - iV_2(\rho_{33} - \rho_{11}) \ , \tag{9d}$$

$$\frac{\partial \tilde{\rho}_{32}}{\partial t} = -\left[\frac{1}{T_2} - i\Delta\right]\tilde{\rho}_{32} - iV_1\tilde{\rho}_{31} + iV_2\tilde{\rho}_{12} \ , \tag{9e}$$

$$\frac{\partial \tilde{\rho}_{21}}{\partial t} = -\left[\frac{1}{T_2} + i\Delta_1\right]\tilde{\rho}_{21} - iV_1(\rho_{22} - \rho_{11}) - iV_2\tilde{\rho}_{23} \ , \tag{9f}$$

where $\rho_{ii}^{\rm eq}$ is the population of level $|i\rangle$ in the absence of the external field and it is assumed that $\rho_{11}^{\rm eq} = 0.5$, $\rho_{22}^{\rm eq} = 0.3$, and $\rho_{33}^{\rm eq} = 0.2$.

The three-level system is formed by the hyperfine levels of the nitrogen nuclear spin $I = 1$ and the two near-resonance fields drive the $\Delta I = \pm 1$ transitions. The two transitions are equivalent and will have, at least to first order, the same longitudinal and transverse relaxation times. The relaxation times have been measured for the $I_z = |0\rangle \Longleftrightarrow |-1\rangle$ transition at 5.4 MHz and the values are $T_1 = 1.2$ ms and $T_2 = 0.4$ ms, which are used in the theoretical calculation [33]. The relaxation times associates with the $\Delta I = 2$ magnetic dipole forbidden transition of $I_z = |1\rangle \Longleftrightarrow |-1\rangle$ at 0.7 MHz are largely determined

by those of the allowed transitions; hence the relaxation times will be of the same magnitude as those associated with allowed $\Delta I=\pm 1$ transitions. Therefore, the same values are used in the calculations and our calculation has shown that the moderate modifications of these values has a negligible effect on the overall line shape.

Under the steady-state limit Eq. (9) can be solved analytically by setting the time derivatives equal to zero. With lengthy algebraic manipulation the solutions are found to be of the form

$$\rho_{22}=\rho_{22}^{eq}+2T_1V_1\,\mathrm{Im}\tilde{\rho}_{21}\ , \tag{10a}$$

$$\rho_{33}=\rho_{33}^{eq}+2T_1V_2\,\mathrm{Im}\tilde{\rho}_{31}\ , \tag{10b}$$

$$\rho_{11}=1-\rho_{22}-\rho_{33}\ , \tag{10c}$$

$$\tilde{\rho}_{31}=\mathrm{Re}\tilde{\rho}_{31}+i\,\mathrm{Im}\tilde{\rho}_{31}\ , \tag{10d}$$

$$\tilde{\rho}_{21}=\mathrm{Re}\tilde{\rho}_{21}+i\,\mathrm{Im}\tilde{\rho}_{21}\ , \tag{10e}$$

$$\tilde{\rho}_{32}-\mathrm{Re}\tilde{\rho}_{32}+i\,\mathrm{Im}\tilde{\rho}_{32} \tag{10f}$$

and

$$\mathrm{Im}\tilde{\rho}_{31}=\frac{w_1V_2(\rho_{11}^{eq}-\rho_{33}^{eq})-y_1V_1(\rho_{11}^{eq}-\rho_{22}^{eq})}{x_1w_1-y_1z_1}\ , \tag{11a}$$

$$\mathrm{Im}\tilde{\rho}_{21}=\frac{x_1V_1(\rho_{11}^{eq}-\rho_{22}^{eq})-z_1V_2(\rho_{11}^{eq}-\rho_{33}^{eq})}{x_1w_1-y_1z_1}\ , \tag{11b}$$

$$\mathrm{Im}\tilde{\rho}_{32}=x\,\mathrm{Im}\tilde{\rho}_{21}+y\,\mathrm{Im}\tilde{\rho}_{31}\ , \tag{11c}$$

$$\mathrm{Re}\tilde{\rho}_{32}=z\,\mathrm{Im}\tilde{\rho}_{21}+w\,\mathrm{Im}\tilde{\rho}_{31}\ , \tag{11d}$$

$$\mathrm{Re}\tilde{\rho}_{31}=\Delta_2T_2\,\mathrm{Im}\tilde{\rho}_{31}+V_1T_2\,\mathrm{Im}\tilde{\rho}_{32}\ , \tag{11e}$$

$$\mathrm{Re}\tilde{\rho}_{21}=\Delta_1T_2\,\mathrm{Im}\tilde{\rho}_{21}-V_2T_2\,\mathrm{Im}\tilde{\rho}_{32}\ , \tag{11f}$$

where Im and Re denote the imaginary and the real part of the complex function, respectively, and we have defined the quantities

$$x=(2\Delta_1-\Delta_2)\frac{V_2}{D}\ , \tag{12a}$$

$$y=(\Delta_1-2\Delta_2)\frac{V_1}{D}\ , \tag{12b}$$

$$z=[1+T_2^2(V_1^2+V_2^2-\Delta\Delta_1)]\frac{V_2}{DT_2}\ , \tag{12c}$$

$$w=[1+T_2^2(V_1^2+V_2^2+\Delta\Delta_2)]\frac{V_1}{DT_2}\ , \tag{12d}$$

$$D=\frac{1}{T_2^2}+V_1^2+V_2^2+\Delta^2\ , \tag{12e}$$

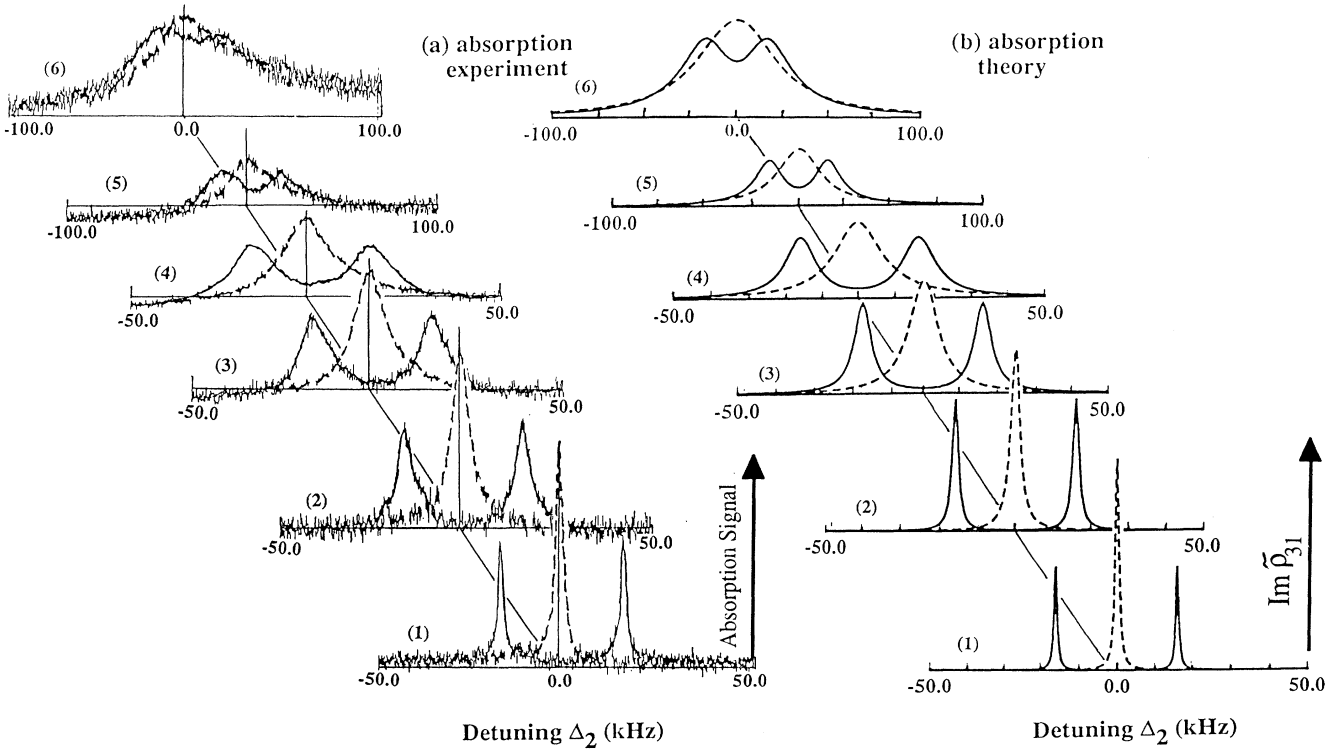

FIG. 3. (a) Experimental and (b) theoretical absorption profile dependence on probe field intensity. The pump field is on resonance with the 4.7-MHz $I_z=|0\rangle \Longleftrightarrow |1\rangle$ transition and has a Rabi frequency of 32 kHz (solid line) and zero (dashed line). The probe field intensities used in experiments are (1) 0 dB ($I=1.0$), (2) 10 dB ($I=10.0$), (3) 20 dB ($I=100.0$), (4) 25 dB ($I=316.2$), and (5) 30 dB ($I=1000.0$), and (6) 35 dB ($I=3162.3$), respectively. The parameters used in theoretical calculation are $T_1=1.2$ ms, $T_2=0.4$ ms, pump field Rabi intensity $\chi_1=32$ kHz, and probe field Rabi intensities χ_2 are (1) 0.26, (2) 0.82, (3) 2.6, (4) 4.62, (5) 8.22, and (6) 14.62 kHz.

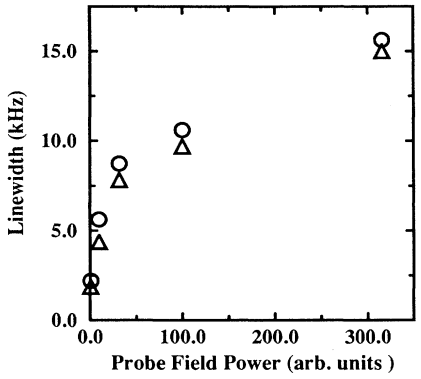

FIG. 4. The linewidth of Autler-Townes doublet (triangle) and the 5.4-MHz transition (circle) dependence on the probe field intensity.

$$x_1=\frac{1}{T_2}+4V_2^2T_1+V_1w+\Delta_2T_2(\Delta_2+V_1y)\ , \tag{12f}$$

$$y_1=V_1(z+xT_2\Delta_2+2T_1V_2)\ , \tag{12g}$$

$$z_1=V_2(w-yT_2\Delta_1+2T_1V_1)\ , \tag{12h}$$

$$w_1=\frac{1}{T_2}+4V_1^2T_1+V_2z+\Delta_1T_2(\Delta_1-V_2x)\ . \tag{12i}$$

The absorptive and dispersive responses of the applied rf fields are proportional to the imaginary and real parts of the off-diagonal density matrix terms $\tilde{\rho}_{31}$ and $\tilde{\rho}_{21}$ [1,2,27]. Since the above solutions are correct to all orders of both fields there is no difference between the pump and the probe field. In the experiment the field of frequency ω_1 is held fixed in frequency resonant with the transition $|1\rangle \Longleftrightarrow |2\rangle$, while the other field is scanned in frequency through the transition $|1\rangle \Longleftrightarrow |3\rangle$. In such a situation the fixed frequency field is called the pump field and the scanned frequency field the probe field. The calculated absorptive and dispersive probe profiles are obtained by plotting $\mathrm{Im}\tilde{\rho}_{31}$ and $\mathrm{Re}\tilde{\rho}_{31}$ as a function of the detuning Δ_2. The amplitude signal corresponds to the magnitude of $|\rho_{31}|=[(\mathrm{Im}\tilde{\rho}_{31})^2+(\mathrm{Re}\tilde{\rho}_{31})^2]^{1/2}$. The results of these calculations are given in Figs. 3, 5, and 6 for a specific pump field intensity and a range of probe field intensities matching experimental conditions. For these calculations the value of $T_1=1.2$ msec and $T_2=0.4$ msec determined experimentally for the 5.4-MHz transition were used. As noted in an earlier paper [1], the transition exhibits only a small amount of inhomogeneous broadening and can be neglected whenever at least one of the Rabi frequencies is larger compared with the inhomogeneous linewidth. Here the traces are obtained for a pump Rabi frequency >30 kHz, which is substantially

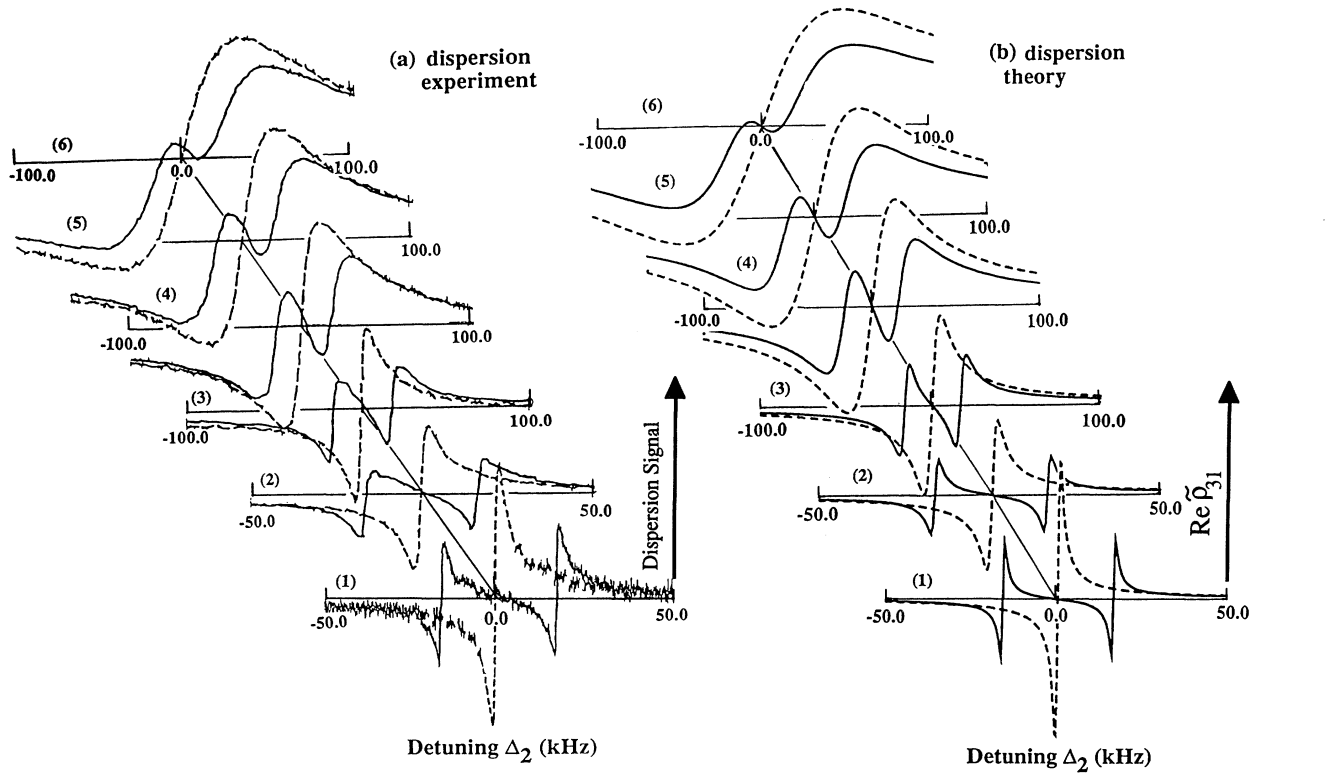

FIG. 5. (a) Experimental and (b) theoretical dispersion profiles dependence on probe field intensity. The pump field is on resonance with the 4.7-MHz $I_z=|0\rangle \Longleftrightarrow |1\rangle$ transition and has a Rabi frequency of 32 kHz (solid line) and zero (dashed line). The probe field intensities used in experiments are (1) dB, ($I=1.0$), 92) 10 dB ($I=10.0$), (3) 20 dB ($I=100.0$), (4) 30 dB ($I=1000.0$), (5) 35 dB ($I=3162.3$), and (6) 40 dB ($I=10\,000.0$), respectively. The parameters used in theoretical calculation are $T_1=1.2$ ms, $T_2=0.4$ ms, pump field Rabi intensity $\chi_1=32$ kHz, and probe field Rabi intensities χ_2 are (1) 0.26, (2) 0.82, (3) 2.6, (4) 8.22, (5) 14.62, and (6) 26 kHz.

larger than the inhomogeneous linewidth of ~2.4 kHz and hence meet the condition.

V. RESULTS AND DISCUSSIONS

A series of experimental absorptive profiles of the 5.4-MHz $I_z=|0\rangle \Longleftrightarrow |-1\rangle$ transition with increasing probe field intensities is shown in Fig. 3(a). The traces of dashed lines are those in the absence of the pump field and represent the power broadening of the transition probed by a single field. The traces of solid lines give the equivalent responses when there is also a pump field applied on resonance with the 4.7-MHz $I_z=|0\rangle \Longleftrightarrow |1\rangle$ transition with a fixed Rabi frequency of $\chi_1=32$ kHz. The probe field intensities used were 0, 10, 20, 25, 30, and 35 dB, respectively. At the "weak probe" limit (0 dB) the absorption line has a linewidth of ~2.4 kHz and shows the well-known symmetric Autler-Townes splitting under on-resonance pumping. As the probe field intensity increases, it interacts nonlinearly with the three-level system and power broadening as well as saturation of the Autler-Townes doublet is observed, as shown in traces (2)–(6) in Fig. 3.

The power broadening behavior of the Autler-Townes doublet (triangle) is shown in Fig. 4. The power broadening of the 5.4-MHz transition itself (circle) is also shown in Fig. 4. It is seen that the power broadening behavior of the Autler-Townes doublet is similar to that of the original transition. The interesting observation is that power broadening for both cases at a high power limit is slower than that predicted by the Bloch equation, consistent with observations in other systems [34,35]. In this paper this aspect will not be investigated further.

The equivalent theoretical absorptive profiles for a pump Rabi frequency of 32 kHz calculated by plotting $\mathrm{Im}\tilde{\rho}_{31}$ as a funciton of detuning Δ_2 are shown in Fig. 3(b). The pump field ω_1 is on resonance with $|1\rangle \Longleftrightarrow |2\rangle$ transition ($\Delta_1=0$). The Rabi intensities of the probe power used in the calculation are $\chi_2=0.26$, 0.82, 2.6, 4.62, 8.22, and 14.62 kHz corresponding to the probe powers 0, 10, 20, 25, 30, and 35 dB, respectively, in the experimental traces of Fig. 3(a). In the experiment the rf field intensity could be obtained by measuring the current in the rf coil. However, it is more appropriate to use the experiment itself as the pump field Rabi intensity can be obtained from the Autler-Townes splitting of the 5.4-MHz transition. The probe field Rabi intensity can be obtained from the splitting of the 4.7-MHz transition or from the power broadening. Such a procedure is followed at one power level and the Rabi intensities at other power levels are obtained by scaling from the known relationship $\chi_2 \propto (\text{probe power})^{1/2}$. The theoretical calcula-

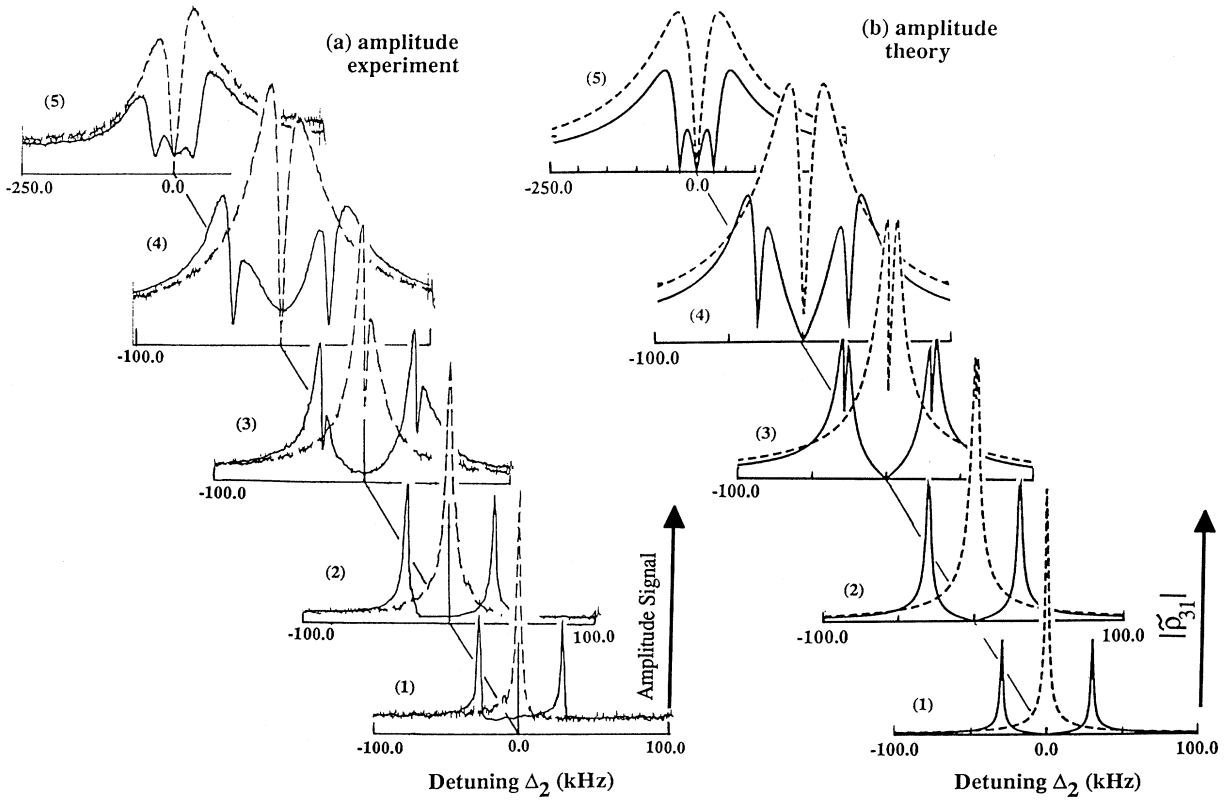

FIG. 6. (a) Experimental and (b) theoretical amplitude profiles dependence on probe field intensity. The pump field is on resonance with the 4.7-MHz $I_z=|0\rangle \Longleftrightarrow |1\rangle$ transition and has a Rabi frequency of 60 kHz (solid line) and zero (dashed line). The probe field intensities used in experiments are (1) 0 dB ($I=1.0$), (2) 10 dB ($I=10.0$), (3) 20 dB ($I=100.0$), (4) 30 dB ($I=1000.0$), and (6) 40 dB ($I=10\,000.0$), respectively. The parameters used in theoretical calculation are $T_1=1.2$ ms, $T_2=0.4$ ms, pump field Rabi intensity $\chi_1=60$ kHz, and probe field Rabi intensities χ_2 are (1) 0.2, (2) 0.632, (3) 2.0, (4) 6.32, and (6) 20.0 kHz.

tion using this procedure gives very good agreement with experiment.

Figure 5(a) shows the experimental dispersive profiles of the 5.4-MHz $I_z=|0\rangle \Longleftrightarrow |-1\rangle$ transition of increasing probe field intensity without (dashed line) and with a driving field (solid line). The driving field is the same as for Fig. 3, which is on resonance with the 4.7-MHz $I_z=|0\rangle \Longleftrightarrow |1\rangle$ transition with a fixed Rabi frequency of $\chi_1=32$ kHz. The probe field intensities used were 0, 10, 20, 30, 35, and 40 dB. It can be seen that the inner parts of the two components of the dispersive doublet which are close to resonance frequency have opposite phase and as the probe field intensity increases, the doublet becomes power broadened and two components interfere destructively with each other. The dispersion profiles continue to grow in size for the probe power used in our experiments.

The theoretical dispersive profiles calculated from $\mathrm{Re}\tilde{\rho}_{31}$ as a function of detuning Δ_2 are shown in Fig. 5(b). The Rabi intensities of the probe power used in the calculation are $\chi_2=0.26$, 0.82, 2.6, 8.22, 14.62, and 26 kHz corresponding to the probe powers 0, 10, 20, 30, 35, and 40 dB, respectively, in the experimental traces of Fig. 5(a). The theoretical calculations give very good agreement with experiment and confirm the various characteristic behaviors, such as power broadening and destructive interference.

The profiles obtained using amplitude detection for increasing probe field intensity are shown in Fig. 6. In this case a higher pump Rabi intensity of 60 kHz is used. The pump field is on resonance with the 4.7-MHz $I_z=|0\rangle \Longleftrightarrow |1\rangle$ transition. As before the solid (dashed) lines are with (without) the pump field. The probe intensities used in experiments are 0, 10, 20, 30, and 40 dB. The probe Rabi frequencies used in theoretical calculation are $\chi_2=0.2$, 0.632, 2, 6.32, and 20 kHz, respectively. It can be seen that the amplitude profiles become power broadened and finally develop into an anomalous line shape with a "hole" in the line center. There is a slight asymmetry in the experimental traces due to a background from the power broadened electron paramagnetic resonance signal [36,37], but allowing for this it can be seen that the calculated profiles are in good agreement with the experimental profiles.

The amplitude signal is the vector sum of absorptive and dispersive components. Since the absorptive response saturates much faster than the dispersive response, the power-broadened dispersive response dominates the amplitude signal at higher power. This point is illustrated more clearly in Fig. 7, where the calculated absorptive, dispersive, and amplitude response are shown [Fig. 7(a)] along with a measured amplitude profile for comparison [Fig. 7(b)]. As phase information is lost in amplitude detection, the negative part of the dispersive response is folded up and results in a rather unusual line shape with a hole in the line center.

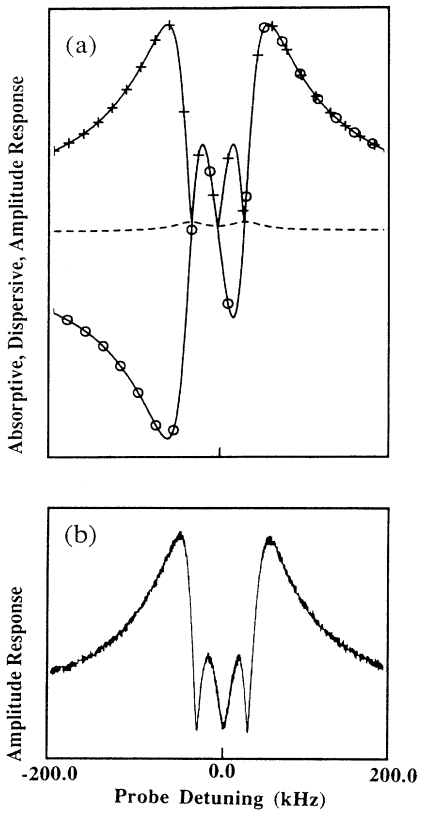

FIG. 7. (a) Schematic showing absorptive (dashed line), dispersive (solid line with circles), and amplitude (solid line with pulses) profiles for high probe field intensity. The different nonlinear behavior of the absorptive and dispersive responses leads to the anomalous amplitude profiles. (b) The experimental amplitude profile is also shown for comparison.

VI. CONCLUSIONS

The power-broadened Autler-Townes doublet profiles in a three-level system subjected to two near-resonance strong electromagnetic fields have been investigated both experimentally and theoretically. The main characteristic noted is that (i) in absorption response the features broadened, saturated, and added constructively, (ii) in dispersion response the features broadened and added destructively, and (iii) in amplitude response the anomalous line shape is observed due to the different saturation behaviors of the absorption and dispersion response at a high power limit. All features are satisfactorily accounted for by a density-matrix treatment for a simple three-level system. The derivation of the density-matrix equation of motion for the three-level system is found in many textbooks [38] and the exact analytical solution for the Λ-shaped three-level system has been derived by Brewer and Hahn [18], whereas the present paper has presented equivalent solutions of the V-shaped three level system.

ACKNOWLEDGMENTS

The authors would like to thank Dr. K. G. Baldwin, Australian National University, Dr. P. T. M. Fisk, M. Sellars, CSIRO (Sydney), and Dr. X.-F. He, University of British Columbia for many helpful discussions.

[1] C. Wei and N. B. Manson, Phys. Rev. A **49**, 4751 (1994).
[2] C. Wei, N. B. Manson, and J. P. D. Martin (unpublished).
[3] X. He, P. T. H. Fisk, and N. B. Manson, J. Appl. Phys. **71**, 211 (1992).
[4] S. H. Autler and C. H. Townes, Phys. Rev. **100**, 703 (1955).
[5] A. Schabert, R. Keil, and P. E. Toschek, Opt. Commun. **13**, 265 (1975).
[6] A. Schabert, R. Keil, and P. E. Toschek, Appl. Phys. **6**, 181 (1975).
[7] C. Delsart and J.-C. Keller, J. Phys. B **9**, 2769 (1976).
[8] Ph. Cahuzac and R. Vetter, Phys. Rev. A **14**, 270 (1976).
[9] J. L. Picque and J. Pinard, J. Phys. B **9**, L77 (1976).
[10] J. E. Bjorkholm and P. F. Liao, Opt. Commun. **21**, 132 (1977).
[11] C. Delsart and J.-C. Keller, J. Phys. (Paris) **39**, 350 (1978).
[12] H. R. Gray and C. R. Storud, Jr., Opt. Commun. **25**, 359 (1978).
[13] C. Delsart and J.-C. Keller, J. Phys. B **13**, 241 (1980).
[14] C. Delsart, J.-C. Keller, and V. P. Kaftandjian, J. Phys. (Paris) **42**, 529 (1981).
[15] P. R. Hammer, B. W. Peuse, F. Y. Wu, J. E. Thomas, and S. Ezekiel, Opt. Lett. **6**, 531 (1981).
[16] P. T. H. Fisk, H.-A. Bachor, and R. J. Sandeman, Phys. Rev. A **33**, 2418 (1986).
[17] P. T. H. Fisk, H.-A. Bachor, and R. J. Sandeman, Phys. Rev. A **34**, 4762 (1986).
[18] R. G. Brewer and E. L. Hahn, Phys. Re . A **11**, 1641 (1975).
[19] S. Feneuille and M.-G. Schweighofer, J. Phys. (Paris) **36**, 781 (1975).
[20] R. M. Whitley and C. R. Stroud, Jr., Phys. Rev. A **14**, 1498 (1976).
[21] W. A. McClean and S. Swain, J. Phys. B **10**, L143 (1977).
[22] C. Cohen-Tannoudji and S. Reynaud, J. Phys. B **10**, 345 (1977).
[23] C. Cohen-Tannoudji and S. Reynaud, J. Phys. B **10**, 2311 (1977).
[24] P. R. Berman and R. Salomaa, Phys. Rev. A **25**, 2667 (1982).
[25] P. T. H. Fisk, H.-A. Bachor, and R. J. Sandeman, Phys. Rev. A **33**, 2424 (1986).
[26] J. Mlynek, N. C. Wong, R. G. DeVoe, E. S. Kintzer, and R. G. Brewer, Phys. Rev. Lett. **50**, 993 (1983).
[27] N. C. Wong, E. S. Kintzer, J. Mlynek, R. G. DeVoe, and R. G. Brewer, Phys. Rev. B **28**, 4993 (1983).
[28] N. B. Manson, P. T. H. Fisk, and X.-F. He, Appl. Magn. Reson. **3**, 999 (1992).
[29] G. Davies and M. F. Hamer, Proc. R. Soc. London Ser. A **348**, 285 (1976).
[30] J. H. N. Loubser and J. A. van Wyk, Diamond Research **11**, 4 (1977).
[31] N. R. S. Reddy, N. B. Manosn, and E. R. Krause, J. Lumin. **38**, 46 (1987).
[32] K. Holliday, N. B. Manson, M. Glasbeek, and E. van Oort, J. Phys. Condens. Matter **1**, 7093 (1989).
[33] C. Wei, Ph.D. thesis, Australian National University, Canberra, 1994.
[34] A. G. Redfield, Phys. Rev. **98**, 1787 (1955).
[35] R. G. DeVoe and R. G. Brewer, Phys. Rev. Lett. **50**, 1269 (1983).
[36] X. He, Ph.D. thesis, Australian National University, Canberra, 1991.
[37] X. He, P. T. H. Fisk, and N. B. Manson, J. Opt. Soc. Am. B **10**, 913 (1993).
[38] For example, see M. Sargent III, M. O. Scully, and W. E. Lamb, Jr., *Laser Physics* (Addison-Wesley, London, 1974); P. Meystre and M. Sargent III, *Elements of Quantum Optics* (Springer, Berlin, 1991).